Neuron

Supplemental Information

Cholinergic Afferent Stimulation Induces Axonal Function Plasticity in Adult Hippocampal Granule Cells

Katiuscia Martinello, Zhuo Huang, Rafael Lujan, Baouyen Tran, Masahiko Watanabe, Edward C. Cooper, David A. Brown, and Mala M. Shah

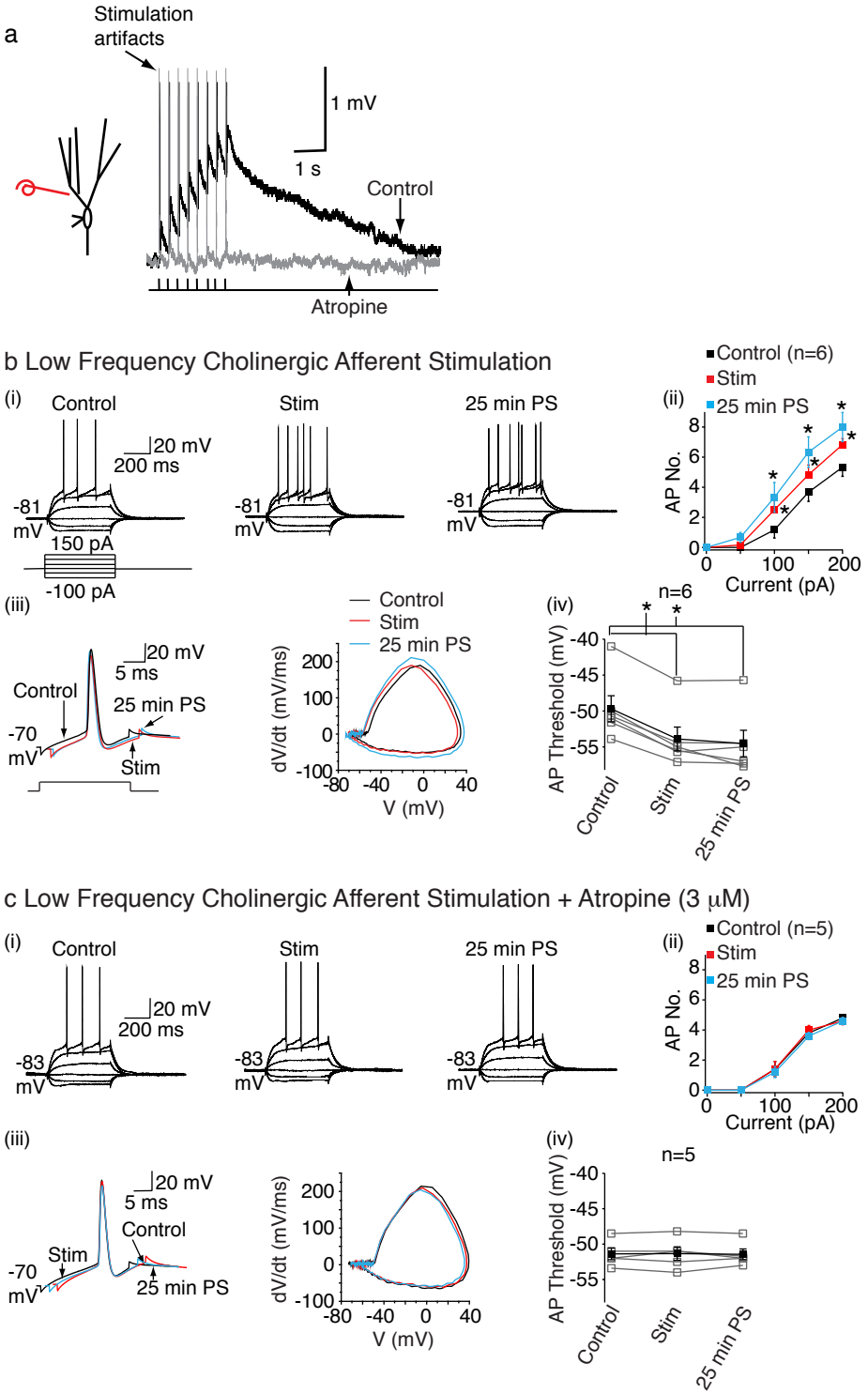

Supp Fig 1 (linked to Fig 1): Intrinsic plasticity induced by low frequency cholinergic afferent stimulation. a Example cholinergic synaptic potentials in the absence (control) and presence of atropine (3 μM). Eight cholinergic synaptic potentials (0.8 Hz; shown in inset) were generated every 325 ms as depicted in the schematic. The stimulation pattern was repeated ten times at 0.1 Hz. **b(i)** and **c(i)** Representative traces obtained in response to a series of 400 ms hyperpolarizing and depolarizing current pulses before, immediately after stimulation (stim) and 25 min post stimulation (PS) in long axon granule cells with and without atropine respectively. The RMP values are indicated adjacent to the traces. The scale shown applies to all traces. **b(ii)** and **c(ii)** Graph depicting the average action potential numbers (AP No.) elicited by depolarizing current steps. **b(iii)** and **c(iii)** Example single action potentials obtained at -70 mV prior, immediately after and 25 min post stimulation in the absence and presence of atropine respectively. The phase plane plots are shown on the right. **b(iv)** and **c(iv)** Individual (open square) and mean (filled squares) action potential threshold values before and after stimulation under control conditions and in the presence of atropine respectively.

Martinello et al. Supp Fig 2

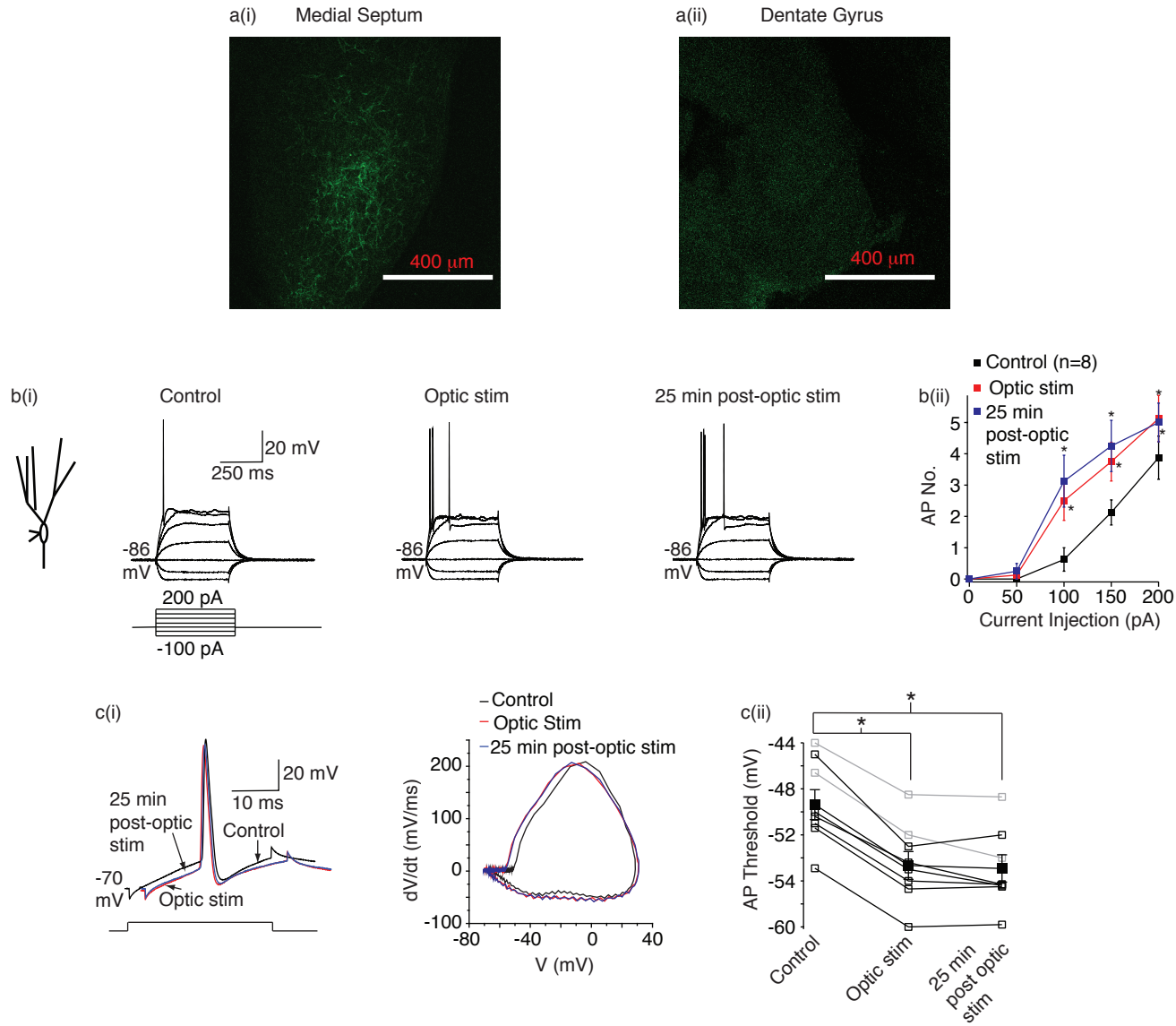

Supp Fig 2: Persistent reduction in spike threshold induced by optical stimulation of cholinergic fibers a(i) Confocal images showing eYFP labelled cholinergic fibers in the medial septum **a(ii)** Confocal images showing eYFP labelled puncta in the dentate gyrus. Both images were taken with same settings and magnification. **b(i)** Example traces recorded from granule cell soma in response to 400 ms long square pulses as indicated in the schematic below before, immediately after and 25 min following optical stimulation (optic stim) of cholinergic fibers in the dentate gyrus region. The RMP values are recorded adjacent to each trace. The scale on the first trace applies to all traces within **b(i)**. **b(ii)** The average numbers of action potentials (AP No.) in response to 400 ms current injections of varying amplitudes. Note that in 6/8 experiments the glutamate and GABA receptor blockers were present. Since there was little difference between experiments in which the blockers were present and those in which they were absent the data were pooled together. **c(i)** Representative single action potentials elicited by a short pulse at -70 mV prior to, immediately after and 25 min post optical stimulation of cholinergic fibers. The associated phase plane plots are shown on the right. **c(ii)** Individual (open squares) and mean (filled square) action potential (AP) threshold values under control conditions and either immediately after or 25 min after optical stimulation of cholinergic fibers. Grey squares represent experiments in which glutamate and GABA receptor blockers were omitted. The data from all experiments irrespective of whether glutamate and GABA receptor blockers were present were pooled together to obtain the mean and SEM values. Asterisks indicate significance at $p < 0.05$.

Martinello et al. Supp Fig 3

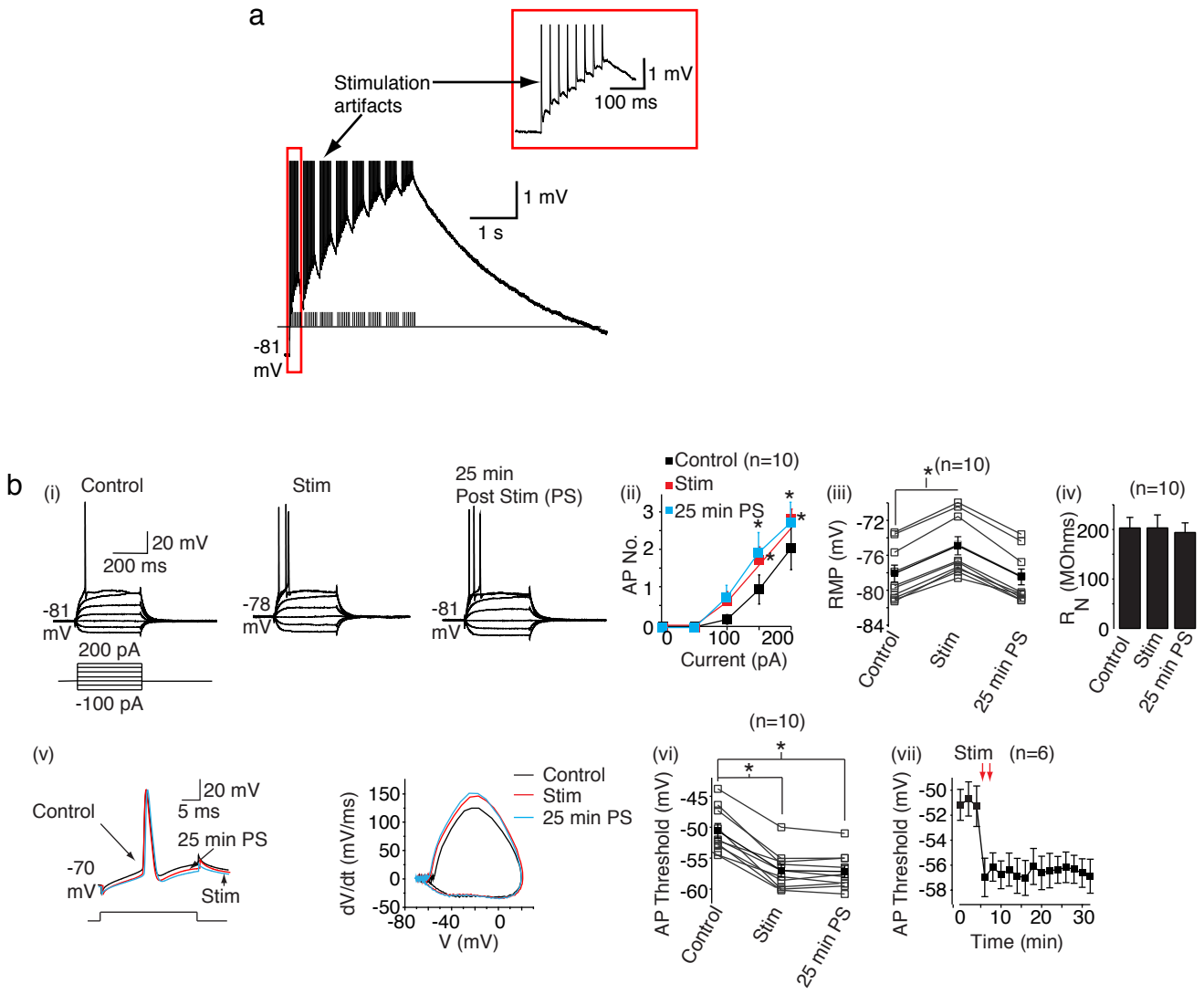

Supp Fig 3 (linked to Fig 1): Neostigmine boosts cholinergic EPSPs and associated action potential threshold plasticity. a Example cholinergic EPSPs obtained by stimulation of cholinergic fibers in the presence of the anticholinersterase inhibitor, neostigmine (3 μM). The inset shows the first burst of EPSPs on an enhanced time scale. **b(i)** Representative traces obtained in response to a series of 400 ms hyperpolarizing and depolarizing current pulses before, immediately after stimulation (stim) and 25 min post stimulation (PS) in long axon granule cells. The RMP values are indicated adjacent to the traces. The scale shown applies to all traces. **(ii)** Graph depicting the average action potential numbers (AP No.) elicited by depolarizing current steps. **(iii)** The individual (open squares) and mean (filled squares) RMP values before, following and 25 min post stimulation. **(iv)** Average input resistance (R_N) values. **(v)** Example single action potentials obtained at -70 mV prior, immediately after and 25 min post stimulation. The associated phase plane plots are shown on the right. **(vi)** Individual (open square) and mean (filled squares) action potential threshold values before and after stimulation. **(vii)** Graph showing the timecourse of the change in action potential threshold values post stimulation.

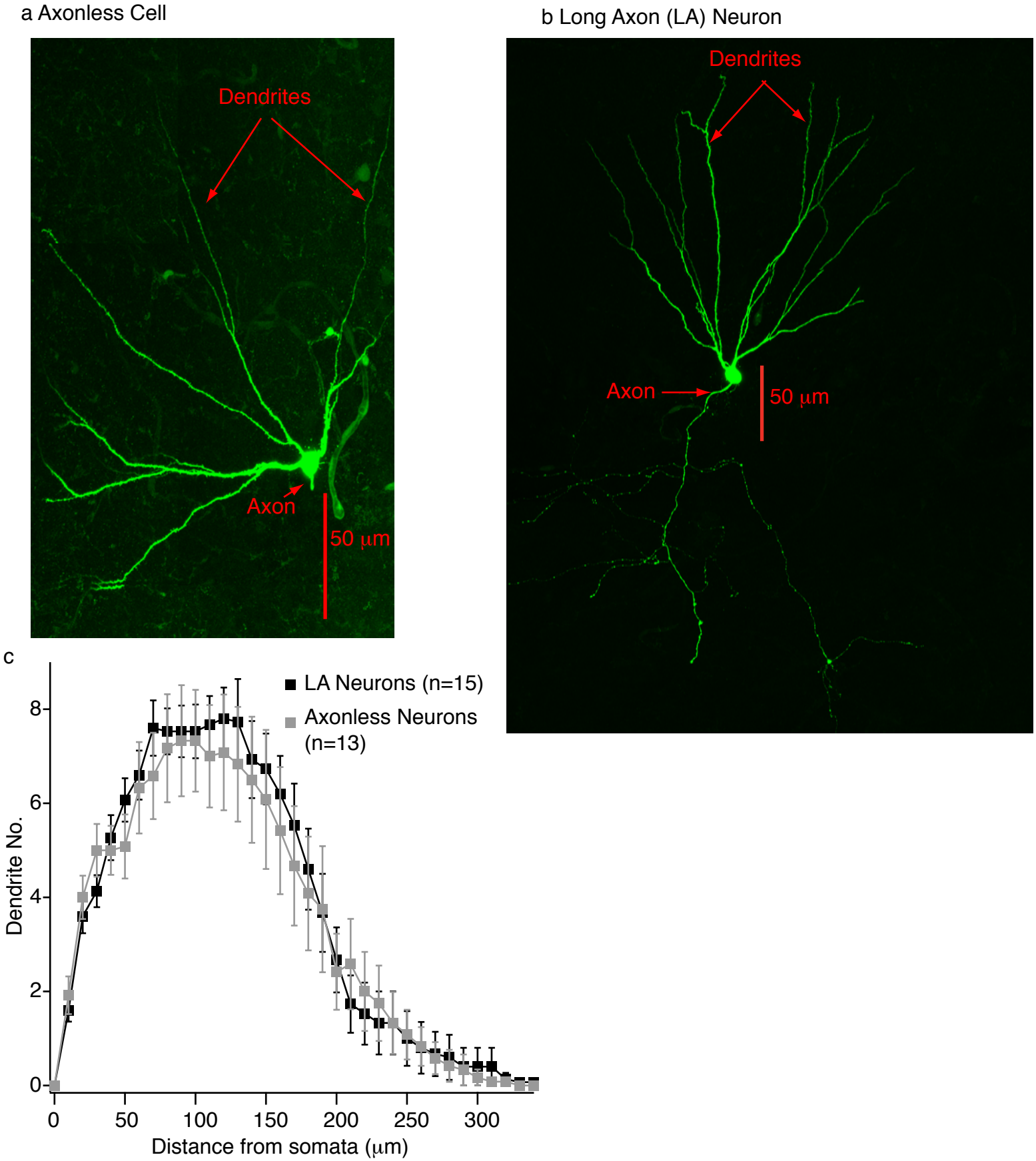

Supp Fig 4 (linked to Fig 2): Sholl analysis of axonless and long axon neuron dendritic trees. a and b Typical images of axonless and long axon neurons respectively obtained using a Zeiss 710 confocal microscope. The neurons had been filled with neurobiotin (2 % w/v), fixed with 4 % paraformaldehyde and stained using streptavidin alexa fluor 488 antibodies. Axonless neurons had an average residual axon length of 6.1 ± 1.2 μm whilst long axon neurons had axons greater than 100 μm long. The images were imported into Image J (NIH) and 10 μm apart concentric circles were constructed around the somata in Image J. The number of dendrites crossing each concentric circle were counted. **c** Plot of the mean and SEM number of dendrites against distance from the somata (Sholl analysis).

Martinello et al. Supp Fig 5

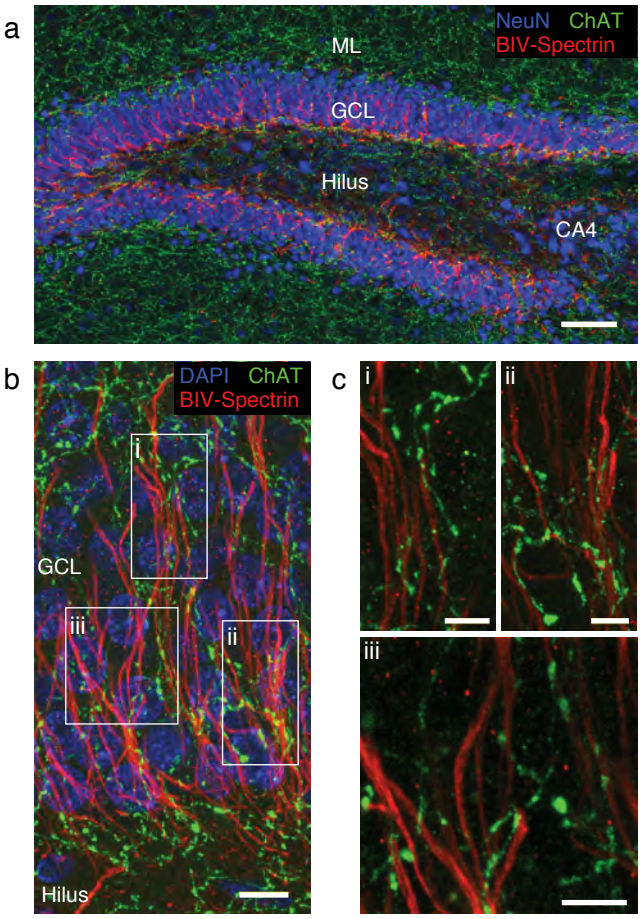

Supp Fig 5: Cholinergic fibers are abundant in the dentate gyrus and lie near granule cell axon initial segments (AISs). a Low magnification image showing cholinergic fibers (ChAT, green) are numerous in the molecular layer **(**ML) and hilus, and more sparse within the granule cell layer (GCL). Cell bodies are labelled with antibodies against the neuron specific protein, NeuN. **b** 15 μm deep maximum intensity projection view of the GCL demonstrating that AISs labelled with βIV spectrin are clustered within columns that are perpendicular to the hilar border. Cell nuclei are labelled with DAPI. Cholinergic fibers detected with ChAT antibodies are enriched within these columns, and sometimes follow the paths of AISs. Boxes enclose regions shown at higher magnification in **c. c** Close proximity of dentate granule cell AISs and ChAT fibers in thin maximal intensity projections ((i)10 μm deep, (ii)15 μm and (iii) 10 μm). Scale bars: a 50 μm; b, 10 μm; c, 5 μm

Martinello et al. Supp Fig 6

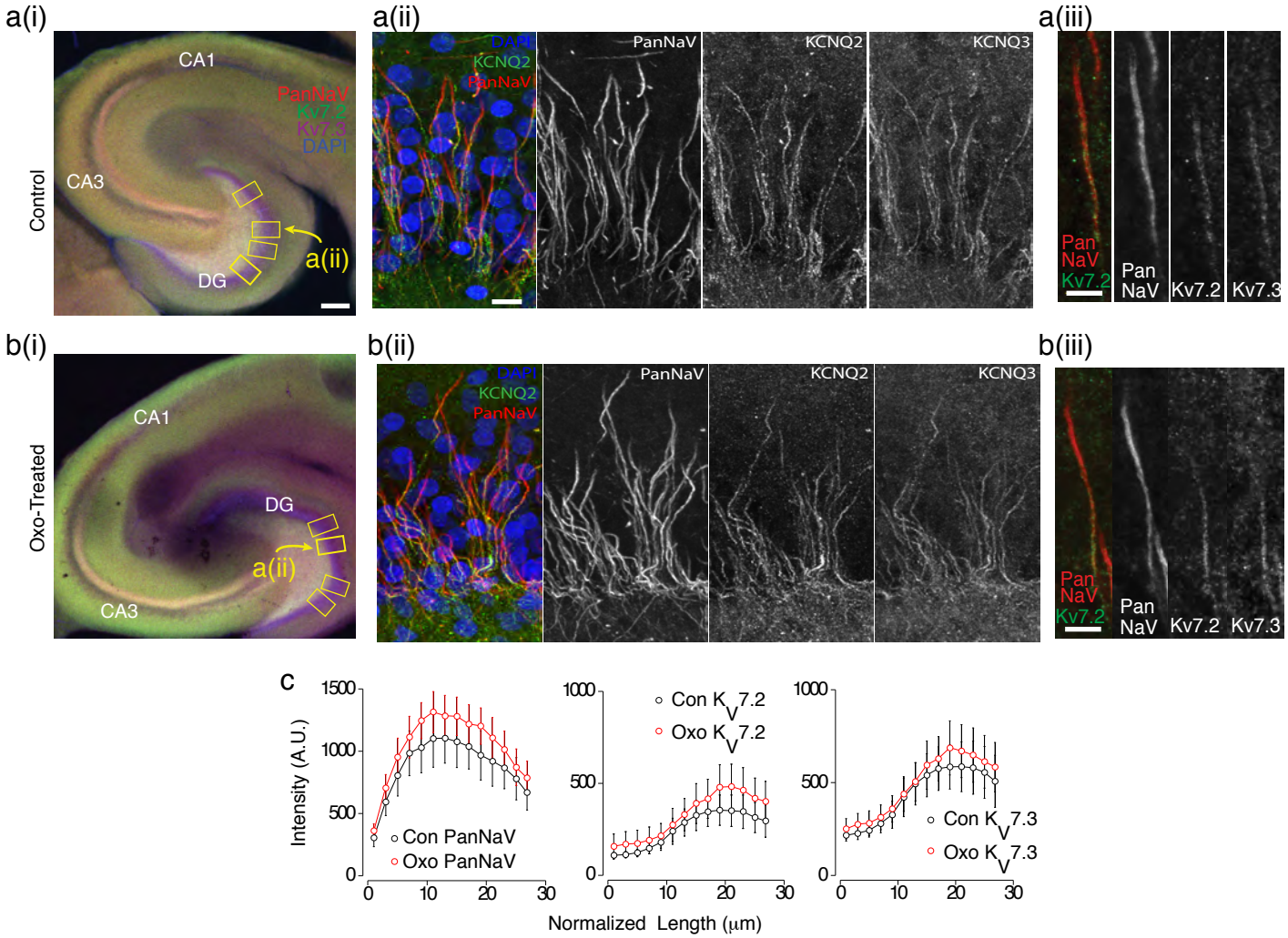

Supp. Fig 6: Na$_V$ and K$_V$7 channel localisation not altered by acute muscarinic receptor stimulation. Example images of p22 -27 rat slices treated for 10 min with either vehicle (control, **a**) or oxotremorine-M (Oxo-M, **b**) labelled with antibodies against NaV (PanNaV), K$_V$7.2 and K$_V$7.3 subunits. The slices were also treated with DAPI to label nuclei of neurons. a(i), b(i) Low magnification images that show labelling for PanNaV, K$_V$7.2 and K$_V$7.3 is most conspicuous along the mossy fiber pathway within the hilus and stratum lucidum of CA3. Boxes show regions of interest (ROIs) where axon initial segment (AIS) labelling intensity was quantified. The ROIs are shown at higher magnification in **a(ii)** and **b(ii)** respectively. **a(iii), b(iii)** Examples of individual AISs in vehicle and Oxo-M treated slices. There is no discernable differences in labelling of K$_V$7.2/7.3 within the AIS between these. **c** Plots of normalised relative intensity of K$_V$7.2/7.3 and PanNaV between control (con; n=3 slices) and Oxo-M (n=3 slices)-treated groups. There is no signficant difference in intensity values within the granule cell AISs between control- and Oxo-M treated groups. Scale bars: **a(i), b(i)**, 100 μm; **a(ii), b(ii)**, 10 μm; **a(iii), b(iii)**, 5 μm. A.U.: arbitrary units.

Martinello et al., Supp Fig 7

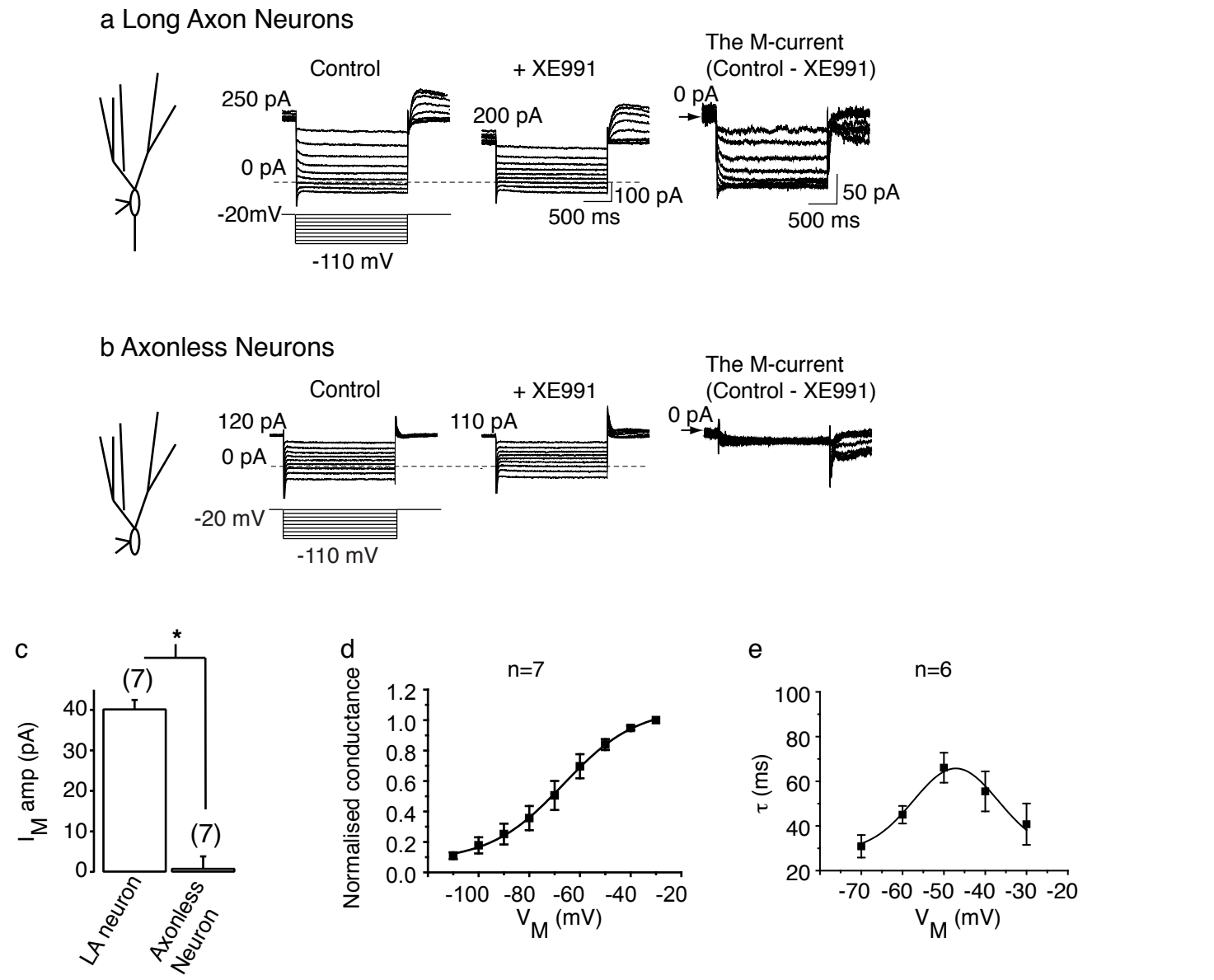

Supp Fig 7 (linked to Fig 3): The M-current is present in long axon neurons but not axonless neurons. a and b. Example de-activating M-current recordings obtained under voltage-clamp conditions using perforated patch-clamp from the somata of granule cells with long axons and axonless neurons respectively in the presence of tetrodotoxin (1 μM), 4-aminopyridine (100 μM) and nickel chloride (1 mM). Cells were held at a fixed potential of -20 mV and 2s hyperpolarizing steps from -30 mV to -110 mV in 10 mV increments were then applied as shown in the schematic. Currents were recorded before (control) and after 15 min bath application of 3 μM XE991. The outward holding currents are indicated on the traces. The scale shown for the raw traces in a applies to all unsubtracted traces in **a** and **b**. The currents obtained in the presence of XE991 were then subtracted from those recorded in the absence to isolate the M-current (far right traces; see **Experimental Procedures**). The scale bars shown for the M-current in **a** apply to that in **b**. Once recordings had been obtained, the patch was ruptured and whole-cell mode achieved to fill the neuron with neurobiotin. Post-hoc morphological analysis was done to verify the axon length. **c** Graph depicting the average M-current amplitude (I_M amp) recorded with a hyperpolarizing step from -20 mV to -50 mV in long axon (LA) and axonless neurons. The numbers of observations for each neuron subtype are shown in parenthesis. **d** The apparent activation curve of the M-current in long axon neurons produced from experimentally derived conductance values. This was constructed using the methods described in Shah et al. (2008, PNAS, 105, 7869). **e**. The average fast de-activation time constants of the M-current recorded at varying voltages (V_M).

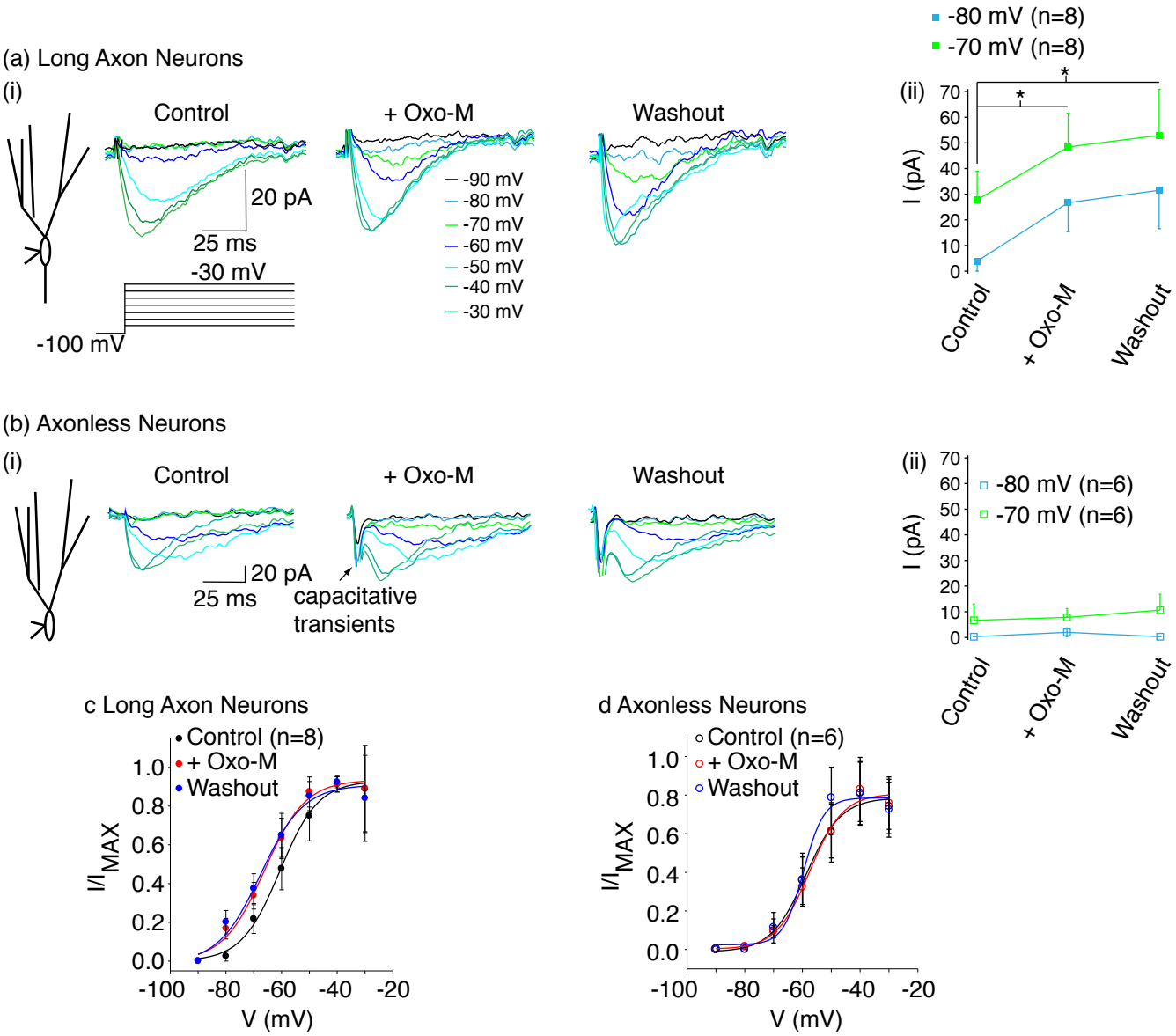

Supp Fig 8: Muscarinic-receptor activation causes sustained enhancement of T-type Ca^{2+} channels. **a(i), b(i)** Example T-type Ca^{2+} currents recorded under control conditions, after 10 min 1 μM Oxo-M application and following 25 min washout of Oxo-M in long axon and axonless neurons respectively. Cells were held at -100 mV and 1 s, depolarizing pulses from -90 mV to -30 mV as shown in the schematic were applied in the absence and presence of TTA-P2 (500 nM). The difference currents (T-type Ca^{2+} currents) are displayed in **a(i)** and **b(i)**. The currents obtained by stepping to -80 mV and -70 mV are shown in blue and green respectively. **a(ii)**, **b(ii)** The amplitude of currents obtained by stepping to -80 mV and -70 mV from -100 mV before, during and 25 min after Oxo-M treatment. **c, d** The activation curves obtained under control conditions, with Oxo-M and after 25 min washout of Oxo-M in long axon and axonless neurons respectively. Asterisks represent significance at $p < 0.05$ compared with controls.

Supp. Table 1 (Linked to Figs 1, 2, 4, 5, 6; see spreadsheet): Comparison of action potential amplitudes and widths following cholinergic stimulation and muscarinic receptor activation. Summary of changes in action potential (AP) amplitude (amp) and width caused by either optical or electrical stimulation of cholinergic axons or by application of Oxo-M in long axon (LA) neurons and axonless neurons. The effects of cholinergic afferent electrical stimulation in the presence of the anticholinesterase inhibitor, neostigmine and the nicotinic receptor blockers, methyllycaconitine (10 nM) and hexamethonium (200 μM) or when atropine (3 μM) was added to the washout are reported. In addition, the effects of either cholinergic fiber electrical stimulation or co-application of Oxo-M and the K_V7 channel inhibitor, XE991, the Ca^{2+} chelator, BAPTA, the water soluble PIP_2 analogue, diC8-PIP_2, or the Ca^{2+} channel inhibitors, cadmium chloride ($CdCl_2$), TTA-P2, nickel chloride ($NiCl_2$) and SNX482 on spike characteritics are shown. The numbers of observations are indicated in parenthesis.

Supp. Table 2 (linked to Figs 1, 2, 4, 5, 6; see spreadsheet): Effects of cholinergic fiber stimulation and Oxo-M on RMP, R_N and ADP in the absence and presence of pharmacological inhibitors. Summary of changes in resting membrane potential (RMP) and input resistance (R_N) when cholinergic fibers were either electrically or optically stimulated at high (27.8 Hz) or low (0.8 Hz) frequency in the absence or presence of the anticholinesterase inhibitor, neostigmine, nicotinic receptor blockers (methyllycaconitine (10 nM) and hexamethonium (200 μM)), the addition of atropine (3 μM) after stimulation, the K_V7 channel inhibitor, XE991 and the T-type Ca^{2+} channel inhibitor, TTA-P2. Also shown are the alterations in RMP and R_N with Oxo-M in long axon (LA) neurons and axonless neurons when bath applied or focally applied either alone or together with XE991, the PIP_2 modulator, diC8-PIP_2, the Ca^{2+} chelator, BAPTA or the Ca^{2+} channel inhibitors, cadmium chloride ($CdCl_2$), TTA-P2, nickel chloride ($NiCl_2$) and SNX482. The effects of these treatments on the area and amplitude of the afterdepolarization induced by Oxo-M application are also reported. Asterisks indicate significant ($p < 0.05$) differences when compared with Oxo-M alone. All effects were reversible upon washout of the compounds. The numbers of observation for each value are indicated in parenthesis.

Martinello et al., 2014, Supp. Table 3 (linked to Fig 2)

	RMP (mV)	R_N (MΩ)
Long Axon Neurons	-80.36 ± 0.2 mV (n=136)	297.94 ± 23.9 (n=117)
Axonless Neurons	-80.14 ± 0.48 mV (n=15)	201.41 ± 15.89 (n=15)

Supp. Table 3: Comparison of intrinsic membrane properties of neurons with and without axons. Table depicting the average resting membrane potential (RMP) and input resistance (R_N) of neurons with intact axons (long axon neurons) and axons with an average axon length of 6.1 ± 1.2 μm (n=18; axonless neurons). The numbers of observations for each parameter are indicated in brackets.

Martinello et al., 2014, Supp. Table 4 (linked to Fig 3)

	Control RMP (mV)	RMP in the presence of modulator (mV)	Control R_N (MΩ)	R_N in the presence of modulator (MΩ)	Control AP amp (mV)	AP amp in the presence of the modulator (mV)	Control AP width (ms)	AP width in the presence of the modulator (ms)
XE991, 3 μM, LA neurons	-80.70 ± 0.97 mV (n=10)	-79.25 ± 1.05 mV (n=10)	251.92 ± 33.0 MΩ (n=10)	264.62 ± 34.0 MΩ (n=10)	74.80 ± 2.88 mV (n=10)	75.29 ± 3.25 mV (n=10)	1.34 ± 0.11 ms (n=10)	1.48 ± 0.09 ms (n=10)
XE991, 3 μM, axonless neurons	-79.68 ± 0.5 mV (n=8)	-80.22 ± 1.15 mV (n=8)	183.01 ± 20.1 MΩ (n=8)	181.85 ± 19.0 MΩ (n=8)	78.39 ± 2.26 mV (n=8)	78.52 ± 1.91 mV (n=8)	1.83 ± 0.09 ms (n=8)	1.9 ± 0.07 ms (n=8)
ABP (8 mM), LA neurons	-80.63 ± 0.53 mV (n=6)	-80.56 ± 0.41 mV (n=6)	348.88 ± 29.8 MΩ (n=6)	373.05 ± 28.3 MΩ (n=6)	75.92 ± 3.94 mV (n=6)	74.13 ± 1.89 mV (n=6)	1.54 ± 0.07 ms (n=6)	1.60 ± 0.04 ms (n=6)
sABP (8 mM), LA neurons	-79.79 ± 0.96 mV (n=8)	-79.83 ± 1.10 mV (n=8)	311.68 ± 33.1 MΩ (n=8)	318.51 ± 33.2 MΩ (n=8)	71.86 ± 1.10 mV (n=8)	70.22 ± 1.94 mV (n=8)	1.35 ± 0.07 ms (n=8)	1.45 ± 0.06 ms (n=8)

Supp. Table 4: Effects of K_V7 channel inhibitors on granule cell intrinsic membrane properties. Comparison of the resting membrane potential (RMP), input resistance (R_N) and action potential (AP) amplitude (amp) and width in the absence (control) and presence of XE991 in long axon (LA) neurons and axonless neurons. The effects of the ankyrin G binding peptide (ABP) and scrambled ABP were also compared. For ABP and sABP, control recordings were those acquired within 2 min of achieving whole-cell mode. Full effects of ABP and sABP occurred within 25 min of achieving whole-cell configuration (**Fig 3**). The numbers of observations for each group are indicated in parenthesis.

Supplementary Movie S1 (linked to Fig 2)

Cholinergic fibers within the granule cell layer are in close proximity to dentate GC AISs. Movie shows a series of images acquired with a z-interval of 0.3 μm. As shown, the GC layer volume is mainly filled by GC somata (NeuN, purple). AISs (primarily from GCs) are clustered in columnar slots between the somata. While the molecular layer and hilus contains a greater overall density of ChAT labeled cholinergic fibers (see Supplementary Fig 3), the ChAT puncta within the GC layer are abundant near the βIV-spectrin labeled AISs (red). Arrows point to examples where cholinergic fibers closely adjoin bundles of AISs. Dimensions (μm): 133.3 w x 61.5 h x 10.5 d.